




Iron and Silicate Dust Growth in the Galactic Interstellar Medium: Clues from Element Depletions

Svitlana Zhukovska¹ , Thomas Henning², and Clare Dobbs³
¹Max-Planck-Institut für Astrophysik, Karl-Schwarzschild-Str. 1, D-85741 Garching, Germany
²Max-Planck-Institut für Astronomie, Königstuhl 17, D-69117 Heidelberg, Germany
³University of Exeter, Stocker Road, Exeter EX4 4QL, UK

Received 2017 August 2; revised 2018 February 25; accepted 2018 February 28; published 2018 April 19

Abstract

The interstellar abundances of refractory elements indicate a substantial depletion from the gas phase, which increases with gas density. Our recent model of dust evolution, based on hydrodynamic simulations of the life cycle of giant molecular clouds (GMCs), proves that the observed trend for $[\text{Si}_{\text{gas}}/\text{H}]$ is driven by a combination of dust growth by accretion in the cold diffuse interstellar medium (ISM) and efficient destruction by supernova (SN) shocks. With an analytic model of dust evolution, we demonstrate that even with optimistic assumptions for the dust input from stars and without destruction of grains by SNe it is impossible to match the observed $[\text{Si}_{\text{gas}}/\text{H}]$ – n_{H} relation without growth in the ISM. We extend the framework developed in our previous work for silicates to include the evolution of iron grains and address a long-standing conundrum: “Where is the interstellar iron?” Much higher depletion of Fe in the warm neutral medium compared to Si is reproduced by the models, in which a large fraction of interstellar iron (70%) is locked as inclusions in silicate grains, where it is protected from efficient sputtering by SN shocks. The slope of the observed $[\text{Fe}_{\text{gas}}/\text{H}]$ – n_{H} relation is reproduced if the remaining depleted iron resides in a population of metallic iron nanoparticles with sizes in the range of 1–10 nm. Enhanced collision rates due to the Coulomb focusing are important for both silicate and iron dust models to match the slopes of the observed depletion–density relations and the magnitudes of depletion at high gas density.

Key words: dust, extinction – Galaxy: abundances – ISM: clouds

1. Introduction

Interstellar dust grains are a small but very important component of the interstellar medium (ISM) of galaxies (Dorschner & Henning 1995). Despite the importance of dust, its main formation route remains a controversial topic. For decades, it was supposed that all refractory grains form in stellar winds of evolved stars and cooling ejecta of supernovae (SNe). In such a formation scenario, however, it is difficult to explain the high depletion of refractory elements in the cold ISM at the level of $\gtrsim 95\%$ for Si and $\gtrsim 99\%$ for Fe for two reasons. First, the timescale of dust formation by stars is longer than the lifetime of grains against destruction in SN shocks (Dwek & Scalo 1980; Jones et al. 1994; Slavin et al. 2015; but see also Jones & Nuth 2011). Second, this scenario requires almost complete condensation of refractory elements in solid form in all matter returned to the ISM by stars. Low- and intermediate-mass stars produce dust efficiently only during the final thermal pulses on the asymptotic giant branch (AGB), while during the preceding evolution on the red giant branch and the first AGB phases stars lose mass efficiently with no or little dust condensation (Gail et al. 2009; McDonald et al. 2011). Moreover, star cluster environment may affect dust condensation and reduce the net dust yield from massive AGB stars (Zhukovska et al. 2015). Similarly, it is unlikely that all refractory elements ejected by core-collapse SNe are in solid form. Although recent observations reveal that grains can form efficiently in expanding SN ejecta (Barlow et al. 2010; Gomez et al. 2012; Indebetouw et al. 2014; Bevan et al. 2016; de Looze et al. 2017), the newly formed dust can be subsequently destroyed by reverse shocks, which substantially reduce the fraction of elements in dust in SN ejecta (Bianchi & Schneider 2007; Silvia et al. 2010; Micelotta et al. 2016).

These discrepancies are resolved in one-zone dust evolution models by assuming that the dust mass can grow in the ISM by gas–grain interactions (Dwek & Scalo 1980; Dwek 1998; Draine 2009). This mechanism of dust formation is also required by very recent dust evolution models based on hydrodynamical simulations of the ISM to match observed dust properties in galaxies (Bekki 2015; McKinnon et al. 2016; Zhukovska et al. 2016; Aoyama et al. 2017).

Direct evidence that metals go in and out of dust in the ISM comes from the observed variations of interstellar element depletions. For instance, the fractions of Si and Fe in the gas decrease by almost 10 times between the warm and cold clouds in the galactic disk (Savage & Sembach 1996). These differences are explained by simple dust evolution models based on idealized two- or three-phase models of the ISM in which grains are destroyed by SN shocks in the intercloud medium and accrete gas-phase elements in clouds; denser gas enriched with dust is exchanged with dust-poor gas during the interstellar matter cycle (Draine 1990; O’Donnell & Mathis 1997; Tielens 1998; Weingartner & Draine 1999). These models are, however, sensitive to the adopted scheme and timescales of mass exchange between ISM phases, which are treated as free parameters.

Using realistic hydrodynamic numerical simulations, Peters et al. (2017) demonstrate that dust grains experience complex evolution in a multiphase ISM characterized by large scatter in the phase exchange timescales. Their work underlines the importance of combining dust models with numerical simulations of the ISM, which incorporate a wide range of physical conditions. Moreover, dust evolution models based on simulations can address a strong observed correlation of element depletions with the average gas density on the line of sight (Savage & Bohlin 1979). Recently, Zhukovska et al.

(2016, hereafter ZDJ16) have presented a new dust evolution model based on hydrodynamic simulation of giant molecular clouds (GMCs) in a Milky-Way-like galaxy, whose resolution is sufficiently high to explore the dependence of interstellar Si depletions on local physical conditions and for the first time compare them with the observational data. They find that a combination of selective accretion of Si on silicate grains in the cold neutral medium (CNM) and dust destruction by interstellar shocks in the diffuse gas are necessary to explain the observed relation between Si depletion and density. In this work, we demonstrate with an analytical model that dust input from stellar sources cannot describe this relation, even with optimistic assumptions for dust condensation efficiencies in stars.

Iron represents a curious test case to investigate dust growth in the ISM with the evolution model developed in our previous work (ZDJ16). In contrast to Si, it is more heavily depleted in the warm neutral medium (WNM) and, because of its comparable abundance to Si and Mg, can be an important component of interstellar dust. Dwek (2016) argues that, with the current observational data for iron dust input from various stellar sources, the observed Fe depletion can be explained only by accretion of gas-phase Fe on grains. The question “In which solid form is the interstellar iron?” poses a long-standing conundrum. The composition of interstellar silicates is not uniquely constrained by the observational data (e.g., Zubko et al. 2004); therefore, the fraction of iron locked in silicates is unclear. Schalen (1965) suggested that the depleted cosmic Fe can be in the form of metallic iron, which unfortunately does not have extinction features for its unambiguous identification. Ossenkopf et al. (1992) include iron both in the silicate lattice and as small inclusions (pure iron and iron oxides) to the silicates to explain the large absorptivity of interstellar dust at the near-infrared wavelengths. Among other solid forms of iron considered in the literature are oxides (Henning et al. 1995; Draine & Hensley 2013), metallic needles (Dwek 2004), iron and FeS inclusions in silicate grains (Min et al. 2007; Jones et al. 2013), an inner layer in multilayered particles (Voshchinnikov et al. 2017), free-flying iron nanoparticles (Gioannini et al. 2017; Hensley & Draine 2017), and hydrogenated iron nanoparticles (Bilalbegovic et al. 2017). Indeed, in situ studies of interstellar dust grains demonstrate that silicate particles contain iron and that individual iron particles exist (Westphal et al. 2014; Altobelli et al. 2016).

In this work, we extend the framework introduced by ZDJ16 to include iron dust evolution. We fix the ratio of carbon to silicate dust mass and postpone the evolution of carbonaceous dust for future studies. Observational constraints from interstellar element depletions are introduced in Section 2. A relation between Si gas-phase abundance and gas density is interpreted with an analytic model of dust evolution in Section 3. We briefly summarize the hydrodynamic numerical simulations of the GMCs and dust evolution model in Section 4.1. Section 4.2 introduces a model for the silicate grains and compares a synthetic relation between the average Si gas-phase abundance and gas density with the observed relation. In Section 4.3, we explore different models for the iron grain population to understand the reasons behind the higher depletion of the interstellar Fe abundance in the WNM compared to the Si depletions and the observed trend of $[\text{Fe}_{\text{gas}}/\text{H}]$ with density. We consider the timescales of physical processes on the grain surface and the role of stochastic heating of small iron grains for the dust growth process in Section 5.

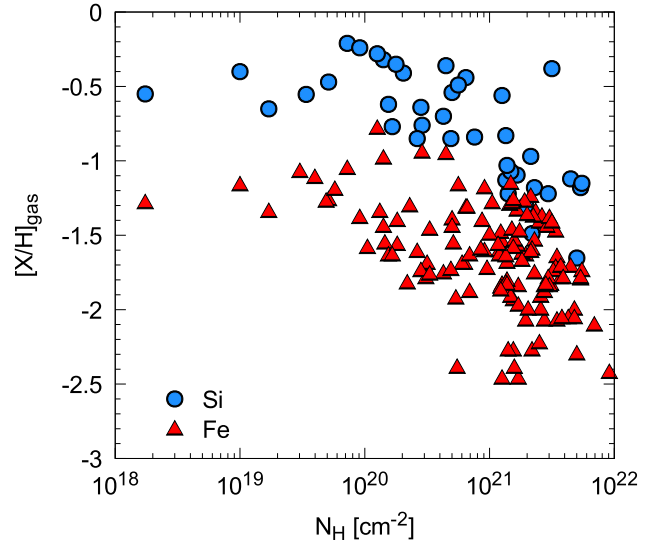


Figure 1. Interstellar element abundances for Si and Fe (circles and triangles, respectively) as a function of hydrogen column density. Observational data are taken from work by Voshchinnikov & Henning (2010).

Discussion of our results is given in Section 6. Finally, our conclusions are presented in Section 7.

2. Gas-phase Si and Fe Depletions

Evolutionary changes in dust composition can be studied by analysis of element depletions in the gas phase measured along various lines of sight, assuming that the elements missing from the gas phase are locked in grains. The logarithmic depletion of an element X in the ISM $[\text{X}/\text{H}]_{\text{gas}}$ is determined as the gas-phase element abundance relative to the reference abundance, for which we adopt its abundance in the Sun:

$$[\text{X}/\text{H}]_{\text{gas}} = \log(N(\text{X})/N(\text{H})) - \log(N(\text{X})/N(\text{H}))_{\odot}, \quad (1)$$

where $N(\text{X})$ refers to the column density of an element X. The linear depletion of element X is, correspondingly,

$$\delta_{\text{X}} = 10^{[\text{X}/\text{H}]_{\text{gas}}}. \quad (2)$$

Abundances of main dust-forming elements in the gas phase decrease with hydrogen column density N_{H} ($N_{\text{H}} = N(\text{H I}) + N(\text{H}_2)$), pointing to the increase of their abundances in dust. Figure 1 demonstrates this observational depletion trend for Si and Fe, which are assumed to be the key elements for silicate and iron dust, respectively. For $N_{\text{H}} > 5 \times 10^{19} \text{ cm}^{-2}$, $[\text{Si}_{\text{gas}}/\text{H}]$ and $[\text{Fe}_{\text{gas}}/\text{H}]$ show similar behavior, despite a 1 dex difference in their values. These changes in the element abundances are driven by dust evolution, which depends on the local gas density rather than on the column density measured observationally. The element depletions have been analyzed in the literature as a function of the averaged gas density along the line of sight, but this quantity can be significantly lower than the actual volume density in a cloud. In our previous work (ZDJ16), we derived a relation between $[\text{Si}_{\text{gas}}/\text{H}]$ and the local gas volume density using fine-structure excitations of neutral carbon from Jenkins & Tripp (2011) measured for 87 lines of sight. The volume density represents local physical conditions of interstellar gas; therefore, the relation between $[\text{Si}_{\text{gas}}/\text{H}]$ and the volume gas density is more suitable to constrain three-dimensional dust evolution models

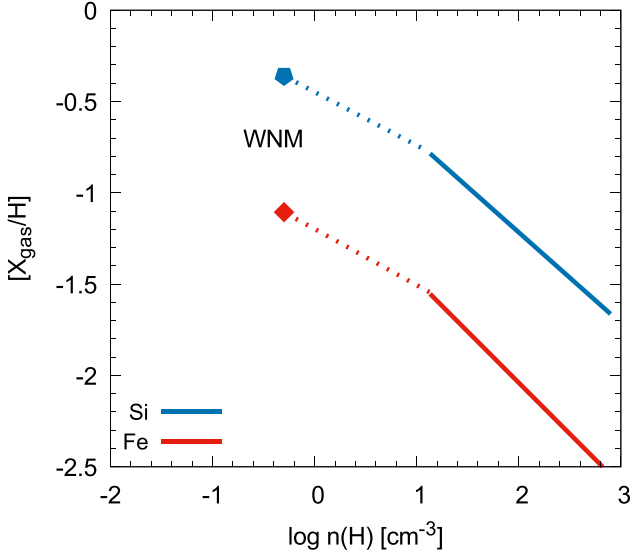


Figure 2. Relations between element depletion and gas density for Si and Fe derived from the least-squares linear fit to observational data (blue and red solid lines, respectively) described in Section 2. The pentagon and diamond show the depletion values for Si and Fe, respectively, in the WNM. Dashed lines are interpolations between the observed values in the WNM and the linear fit relations.

than the relation for the average density on the line of sight. We find that $[\text{Si}_{\text{gas}}/\text{H}]$ correlates with the gas density as $n_{\text{H}}^{-0.5}$.

To derive the analogous relation between $[\text{Fe}_{\text{gas}}/\text{H}]$ and n_{H} , we combine the relation for Si given by Equation (20) from ZDJ16 and Equation (10) from Jenkins (2009) with coefficients for Si and Fe. The resulting equation is

$$[\text{Fe}_{\text{gas}}/\text{H}] = -0.56 \log(n_{\text{H}}) - 0.72. \quad (3)$$

The slope of this relation, -0.56 , is slightly steeper than the value of -0.5 for Si, indicating that Fe is more readily depleted from the gas phase than Si (Figure 2).

The gas density range accessible through the C I fine-structure lines is restricted to about $10\text{--}10^3 \text{ cm}^{-3}$. Since the element depletion is measured along the entire line of sight, the resulting $[\text{X}/\text{H}]_{\text{gas}}$ value can be higher than the depletion in a cloud probed by C I because of the contribution of WNM on the same line of sight (see ZDJ16, for details). Although the contamination from the WNM does not have a large effect on the coefficients in the $[\text{Si}_{\text{gas}}/\text{H}]\text{--}n_{\text{H}}$ relation, its magnitude can reach 0.1–0.2 dex for $[\text{Si}_{\text{gas}}/\text{H}]$ (E. B. Jenkins 2018, private communication). To account for this effect, the relations for Si and Fe are shifted downward by 0.2 in Figure 2.

Figure 2 also includes the depletion levels in the WNM at a location for a typical density of the WNM $n_{\text{H}} = 0.5 \text{ cm}^{-3}$. The values $[\text{Fe}_{\text{gas}}/\text{H}] = -1.11$ and $[\text{Si}_{\text{gas}}/\text{H}] = -0.36$ are calculated from Equation (10) in Jenkins (2009) for $F_* = 0.12$ recommended for the WNM. These values are slightly higher than the values $[\text{Fe}_{\text{gas}}/\text{H}] = -1.22$ and $[\text{Si}_{\text{gas}}/\text{H}] = -0.43$ recommended for the warm disk by Savage & Sembach (1996) based on a smaller data sample. Comparison of the depletion values for the WNM and the relations for $[\text{Si}_{\text{gas}}/\text{H}]$ and $[\text{Fe}_{\text{gas}}/\text{H}]$ derived for $n_{\text{H}} \gtrsim 10 \text{ cm}^{-3}$ points to shallower slopes in the density range $0.5\text{--}10 \text{ cm}^{-3}$.

3. Analytic Steady-state Model

3.1. Formulation

In this section, we derive a conceptual model for the fraction of an element X remaining in the gas δ_{X} as a function of the gas density, aiming to explain the observational trends discussed in the preceding section. We adopt a formulation of dust evolution in the solar neighborhood (Zhukovska et al. 2008, hereafter ZGT08) and substantially simplify it assuming a steady-state situation for δ_{X} . This assumption is appropriate to study the present-day element depletions in an evolved galaxy such as the Milky Way. This is a one-zone model, which considers the surface density of dust Σ_{d} averaged over the ISM phases within an annulus at the solar galactocentric radius. The average depletion is related to the dust surface density as

$$\delta_{\text{X}} = 1 - \Sigma_{\text{d}}/\Sigma_{\text{d,max}}, \quad (4)$$

where $\Sigma_{\text{d,max}}$ is the maximum surface density of dust, corresponding to the complete condensation of the key element X. The evolution of Σ_{d} is described by the equation

$$\frac{d \Sigma_{\text{d}}}{dt} = R_{\text{d,inj}} + R_{\text{d,gr}} - \frac{\Sigma_{\text{d}}}{\tau_{\text{SF}}} - \frac{\Sigma_{\text{d}}}{\tau_{\text{d,SN}}}, \quad (5)$$

where $R_{\text{d,inj}}$ is the rate of dust injection by stellar sources, $R_{\text{d,gr}}$ is the growth rate by gas–grain interactions in the ISM, the third and fourth terms on the right-hand side are the rates of dust destruction by star formation and by SN blast waves, respectively, and τ_{SF} and $\tau_{\text{d,SN}}$ are corresponding timescales of these processes. The timescale of star formation is $\tau_{\text{SF}} = \Sigma_{\text{ISM}}/\psi$, where Σ_{ISM} is the surface density of gas and ψ is the star formation rate per unit area. The timescale of dust destruction by SNe is provided by (Dwek & Scalzo 1980)

$$\tau_{\text{d,SN}} = \frac{\Sigma_{\text{ISM}}}{f_{\text{SN}} m_{\text{cl}} R_{\text{SN}}}, \quad (6)$$

where f_{SN} is the fraction of all SNe that destroy dust, m_{cl} is the mass of gas cleared of dust by a single SN, and R_{SN} is the current SN rate. m_{cl} is determined by the material and size distribution of dust grains (Jones et al. 1994). Assuming that only Type II SNe destroy dust, and approximating the SN rate by $R_{\text{SN}} \approx \eta_{\text{SN}} \psi$, where $\eta_{\text{SN}} = 1/150 M_{\odot}$ is the number of SNe per unit of stellar mass formed for the initial mass function (IMF) from Kroupa (2002), we derive the relation between the timescales

$$\tau_{\text{d,SN}} = \frac{\tau_{\text{SF}}}{f_{\text{SN}} m_{\text{cl}} \eta_{\text{SN}}}. \quad (7)$$

We introduce the effective destruction timescale

$$\frac{1}{\tau_{\text{d,eff}}} = \frac{1}{\tau_{\text{SF}}} + \frac{1}{\tau_{\text{d,SN}}} = \frac{1 + f_{\text{SN}} m_{\text{cl}} \eta_{\text{SN}}}{\tau_{\text{SF}}}. \quad (8)$$

The rate of dust injection by stars is approximated as (O’Donnell & Mathis 1997; Weingartner & Draine 1999)

$$R_{\text{d,inj}} = \frac{(1 - \delta_{\text{in}}) \Sigma_{\text{d,max}}}{\tau_{\text{in}}}, \quad (9)$$

where δ_{in} is the fraction of element X left in the gas in matter injected by stars and τ_{in} is the timescale on which stars return matter to the ISM. An accurate expression for $R_{\text{d,inj}}$ including

its dependence on stellar mass and metallicity can be found in ZGT08.

We adopt a model of dust growth in the ISM proposed by ZGT08, in which grains grow by accretion of elements in clouds characterized by the total mass fraction X_{cl} and lifetime τ_{exch} . It allows us to account for the finite time available for the dust growth by accretion before cloud dispersal. The dust growth rate is determined by the parameters of clouds as follows:

$$R_{\text{d,gr}} = \frac{f_{X,\text{ret}} \Sigma_{\text{d,max}} - \Sigma_{\text{d}}}{\tau_{\text{exch,eff}}}, \quad (10)$$

where $\tau_{\text{exch,eff}} = \tau_{\text{exch}}(1 - X_{\text{cl}})/X_{\text{cl}}$ is the effective timescale required for the entire ISM to cycle through the cloud phase and $f_{X,\text{ret}}$ is the fraction of element X condensed in dust in the material returned from clouds. The corresponding depletion is $\delta_{X,\text{ret}} = 1 - f_{X,\text{ret}}$. We employ Equation (32) from ZGT08 for the time evolution of $f_{X,\text{ret}}$ and, assuming that the depletion of gas forming clouds is not too different from the average depletion δ_X , find the depletion at the end of the cloud lifetime ($t = \tau_{\text{exch}}$):

$$\delta_{X,\text{ret}} = 1 - f_{X,\text{ret}} = \frac{\delta_X}{\delta_X + (1 - \delta_X)e^{\tau_{\text{exch}}/\tau_{\text{gr}}}}, \quad (11)$$

where τ_{gr} is the timescale of dust growth by accretion of the key species from the gas phase given by

$$\tau_{\text{gr}}^{-1} = \frac{3\alpha_X A_{X,\text{dust}} m_{\text{amu}}}{\rho_{X,c} \nu_{X,c}} \cdot \frac{1}{\langle a_X \rangle} \cdot v_{X,\text{th}} n_{\text{H}} \cdot \epsilon_X, \quad (12)$$

where α_X is the sticking efficiency to the grain surface, $A_{X,\text{dust}}$ is the atomic weight of one formula unit of the dust species, $\rho_{X,c}$ is the density and $\nu_{X,c}$ is the number of atoms of the key element contained in the formula unit of the condensed phase, $\langle a_X \rangle$ is the average grain radius, $v_{X,\text{th}}$ is the thermal speed of the growth species, and ϵ_X is the element abundance of the key species.

We derive the expression for the evolution of δ_X by differentiating both sides of Equation (4),

$$\frac{d\delta_X}{dt} = \frac{\delta_X - \delta_{\text{in}}}{\tau_{\text{in}}} + \frac{\delta_X - \delta_{\text{ret}}}{\tau_{\text{exch,eff}}} - \frac{(1 - \delta_X)}{\tau_{\text{d,eff}}}. \quad (13)$$

In the derivation of Equation (13), we assumed that $d\Sigma_{\text{d,m}}/dt = \Sigma_{\text{d,m}}/\tau_{\text{in}}$ and used Equation (5) for $d\Sigma_{\text{d}}/dt$, in which the expressions for dust destruction and production rates are rewritten for δ_X with the use of Equation (4). We also used Equation (8) for the total destruction rate. In a steady state, $d\delta_X/dt = 0$, and Equation (13) combined with Equation (11) yields a simple quadratic equation for δ_X ,

$$\delta_X(\tau_{\text{exch,eff}}^{-1} + \tau_{\text{in}}^{-1} + \tau_{\text{d,eff}}^{-1}) - \frac{\delta_X \tau_{\text{exch,eff}}^{-1}}{\delta_X(1 - e^{\tau_{\text{exch}}/\tau_{\text{gr}}}) + e^{\tau_{\text{exch}}/\tau_{\text{gr}}}} - \left(\frac{\delta_{\text{in}}}{\tau_{\text{in}}} + \frac{1}{\tau_{\text{d,eff}}} \right) = 0. \quad (14)$$

The solution of this equation determines δ_X as a function of density and temperature of clouds, for a fixed set of other model

parameters. Assuming that the ISM is an ideal gas in pressure equilibrium, we can replace the temperature dependence in Equation (12) by

$$T_{\text{gas}} = T_0 \frac{n_0}{n_{\text{H}}}, \quad (15)$$

where we adopt the density $n_0 = 30 \text{ cm}^{-3}$ and temperature $T_0 = 100 \text{ K}$ in the idealized CNM for the thermal pressure in the ISM. Then the growth timescale τ_{gr} is

$$\tau_{\text{gr}} = \frac{t_0}{n_{\text{H}}^{0.5}}, \quad (16)$$

where t_0 is the constant determined by the dust properties given by Equation (12).

3.2. Implications for $[\text{Si}_{\text{gas}}/\text{H}] - n_{\text{H}}$ Relation

In the following we compare predictions of the steady-state model for Si depletion $\delta_{\text{Si}}(n_{\text{H}})$ with the observed $[\text{Si}_{\text{gas}}/\text{H}] - n_{\text{H}}$ relation (Section 2), which has been extensively studied with numerical simulations by ZDJ16.

Following ZGT08, we adopt a fixed power-law distribution of grain sizes with the lower and upper size limits of 0.005 and 0.25 μm , respectively, and the power of -3.5 (Mathis et al. 1977, hereafter called MRN). The model parameters in the solar neighborhood are also taken from ZGT08, $f_{\text{SN}} = 0.35$, $\psi = 4 M_{\odot} \text{ pc}^{-2} \text{ Gyr}^{-1}$, $\Sigma_{\text{ISM}} = 10 M_{\odot} \text{ pc}^{-2}$, $X_{\text{cl}} = 0.2$, and, for silicate dust, $t_0 = 87 \text{ Myr}$ and $m_{\text{cl}} = 1500 M_{\odot}$. The dust destruction timescales are then $\tau_{\text{SF}} = 2.5 \text{ Gyr}$, $\tau_{\text{d,SN}} = 0.7 \text{ Gyr}$, and $\tau_{\text{d,eff}} = 0.55 \text{ Gyr}$. For the timescale of dust injection by stars τ_{in} , we adopt an optimistic value of 1 Gyr. Full time-dependent dust evolution models predict much higher values of τ_{in} , exceeding 9 Gyr for the present day (Dwek 1998; ZGT08).

Figure 3 illustrates solutions of Equation (14) for $\log \delta_{\text{Si}} \equiv [\text{Si}_{\text{gas}}/\text{H}]$ for models with and without dust destruction by SN shocks. Grains are destroyed in the process of star formation in all models. We assume complete condensation in stars ($\delta_{\text{in}} = 0$) to evaluate the role of stars for $[\text{Si}_{\text{gas}}/\text{H}]$ distribution in the case of their highest possible contribution. We also show the final depletions $\log \delta_{\text{Si,ret}}$ given by Equation (11) in the matter returned by clouds upon their disruption.

At low gas densities, the dust input rate from stars is higher than the growth rate in the ISM, because the dust growth is inefficient ($\delta_{X,\text{ret}} \simeq \delta_X$) for $\tau_{\text{gr}} \gg \tau_{\text{exch}}$. The Si depletion is therefore determined by the balance between dust input from stars and destruction, which does not depend on n_{H} under our assumptions. Therefore, the $[\text{Si}_{\text{gas}}/\text{H}] - n_{\text{H}}$ relation flattens at lower densities. Despite the assumption of the complete condensation in stars and the short timescale of dust formation by stars, the lowest values of $[\text{Si}_{\text{gas}}/\text{H}]$ provided by stellar sources in models with and without dust destruction in SN shocks are -0.2 and -0.55 , respectively (Figure 3). These values are well above the observed depletions in the CNM.

We also consider a model without dust growth in the ISM, in which we include the dependence of m_{cl} on ambient density considered in Appendix A. In this case, the $[\text{Si}_{\text{gas}}/\text{H}]$ level is determined by the balance between the stardust input and dust destruction in the ISM. Because the m_{cl} decreases with ambient density, this model also produces a negative slope, but it is too shallow compared to observations. The lowest $[\text{Si}_{\text{gas}}/\text{H}]$ value of -0.3 is higher than measurements in the WNM and CNM.

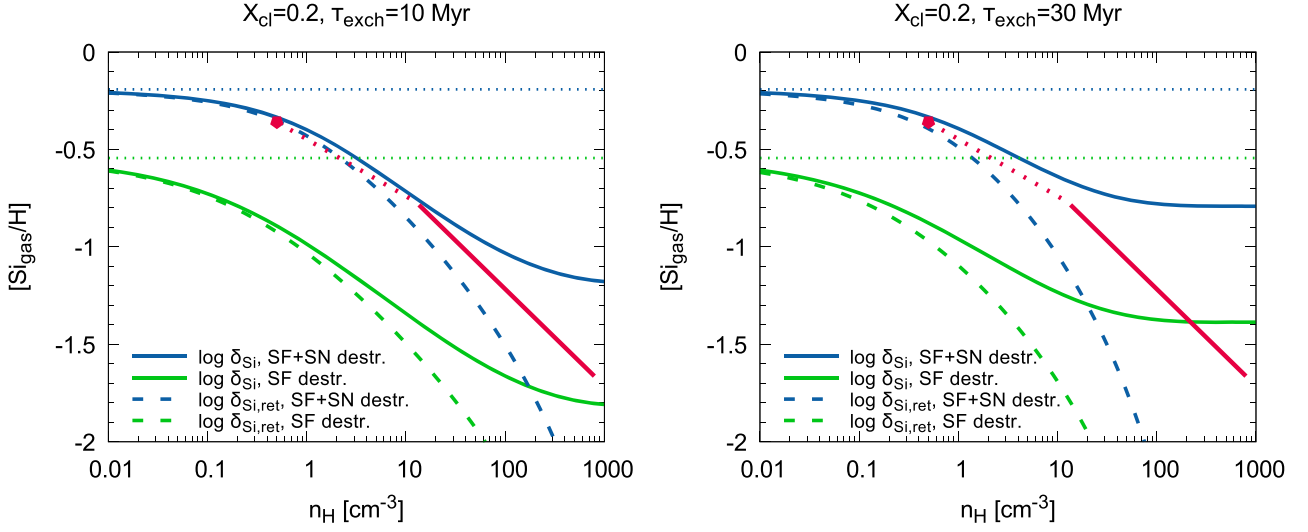


Figure 3. Si gas abundance $[Si_{\text{gas}}/H] \equiv \log \delta_{Si}$ predicted by a simple steady-state model as a function of the gas density in clouds n_H (solid lines). Left and right panels show results for the lifetime of clouds of 10 and 30 Myr, respectively. Blue and green lines are for cases with and without dust destruction in SN shocks, respectively. Dashed lines demonstrate the final depletion $\log \delta_{Si,ret}$ in the matter returned by clouds upon disruption. Depletion levels in models without dust growth in the ISM are shown with dotted lines. The observational data for Si are the same as in Figure 2.

With the increase of the cloud density, $[Si_{\text{gas}}/H]$ decreases owing to a higher rate of dust growth by accretion in clouds. Models with dust destruction only by star formation over-predict Si depletions for the entire density range. Models with dust destruction by SNe match the observed depletion in WNM and enclose the linear fit to the observational data available for $n_H > 10 \text{ cm}^{-3}$ between the steady-state values of $\log \delta_{Si}$ in the ISM and the maximum depletion reached in clouds $\log \delta_{Si,ret}$. This conclusion holds for the current assumption of the complete condensation in stars and a short timescale τ_{in} . If stars are less efficient in dust formation, the model requires a lower efficiency of dust destruction in shocks (lower m_{cl}).

The shape of the model $[Si_{\text{gas}}/H]-n_H$ relation depends on the residence time of grains in clouds, i.e., the lifetime of clouds in our model. For simplicity, we adopt fixed τ_{exch} values of 10 and 30 Myr for short and long lifetimes of clouds, respectively. The difference between $\log \delta_{Si}$ and $\log \delta_{Si,ret}$ for $\tau_{\text{exch}} = 10$ Myr corresponds to the scatter of observational data of up to 1 dex (see Figure 2 in ZDJ16) but appears too large for $\tau_{\text{exch}} = 30$ Myr. In the dense gas, the growth timescale is shorter than the lifetime of clouds for both adopted values of τ_{exch} ; hence, grains rapidly accrete available metals from the gas long before the matter is released from clouds. A longer τ_{exch} means a delayed enrichment of the ISM with highly depleted gas from clouds, which results in the flattening of the $[Si_{\text{gas}}/H]-n_H$ relation for $n_H \gtrsim 50 \text{ cm}^{-3}$. The observational relation favors the shorter lifetime of clouds of 10 Myr. This lower value is also in better agreement with the residence times in the molecular and cold phases inferred from numerical hydrodynamic simulations by Peters et al. (2017).

The simple steady-state model for $[Si_{\text{gas}}/H]$ explains the observed depletion trend with density as the result of the density dependence of the timescale of dust growth in the ISM. The ~ 1 dex scatter in the observational data is explained by the gradual depletion of Si in the process of dust growth, with the lowest depletions limited by the residence times of grains in clouds.

4. Numerical Simulations

In order to model the element depletions self-consistently and account for the dependence of dust evolution on local physical conditions, one has to solve a time-dependent problem including complex dynamical evolution of gas from numerical hydrodynamic simulations with sufficiently high resolution. In the following we discuss the $[Si_{\text{gas}}/H]-n_H$ relation predicted with such a dust evolution model in an evolving multi-phase ISM.

4.1. Description of the Model

The model presented here is a combination of the hydrodynamical simulations of the ISM in a Milky-Way-like disk and a dust evolution model including dust destruction by SNe and dust growth by accretion of gas-phase metals in the ISM. The detailed description of the model can be found in ZDJ16. It utilizes a smoothed particle hydrodynamics (SPH) simulation of destruction and formation of GMCs in a spiral Milky-Way-like galaxy described in Dobbs & Pringle (2013). The simulation is performed using the SPH code sphNG (Benz et al. 1990; Bate et al. 1995; Price & Monaghan 2007). There are a total of 8 million gas particles, and each one has a mass $m_{\text{SPH}} = 312.5 M_{\odot}$. The gas is situated in a disk with radius of 10 kpc, and the average surface density of the gas is $\Sigma_{\text{gas}} = 8 M_{\odot} \text{ pc}^{-2}$. The total simulation time of 270 Myr permits the system to reach steady state between destruction and growth of dust, which strongly correlates with the life cycle of GMCs. Dust is modeled in a post-processing scheme using histories of the physical conditions from hydrodynamic simulations. Assuming perfect coupling between dust and gas, we model evolution of δ_X in each SPH gas particle. In this paper, we update the model for element Si and extend it to include Fe.

The dust model accounts for the dependence of dust growth by gas-grain collisions on local gas temperature and density. ZDJ16 found that growth of silicate dust is so efficient that it has to be suppressed in the warm medium. Following

ZDJ16, it is limited to gas temperatures below 300 K in this work. Additionally, enhanced collision rates in the CNM due to Coulomb focusing are important to reproduce the observed $[\text{Si}_{\text{gas}}/\text{H}]-n_{\text{H}}$ relation.

The grain size distribution is crucial for dust growth in the ISM, as it determines the total grain surface area. The accretion timescale is proportional to the average grain radius

$$\langle a \rangle_3 = \langle a^3 \rangle / \langle a^2 \rangle, \quad (17)$$

where $\langle a^l \rangle \sim \int dn_{\text{gr}}(a)/da a^l da$ is the l th moment of the grain size distribution, with $dn_{\text{gr}}(a)$ the number of grains with radii from a to $a + da$. The mean grain radius modified by the effect of Coulomb focusing is

$$\langle a^m \rangle_3 = \langle a^3 \rangle / \int dn_{\text{gr}}(a) / da D(a) a^2 da, \quad (18)$$

where the enhancement factor $D(a)$ accounts for the change in the cross section of an interaction between ion and grain (Weingartner & Draine 1999). For neutral particles in MCs, $D(a) = 1$. For simplicity, we adopt the MRN grain size distribution $dn_{\text{gr}}(a)/da \sim a^{-3.5}$ (Mathis et al. 1977) with the lower and the upper limits for the grain sizes a_{min} and a_{max} that differ for iron and silicate grains.

The rate of dust destruction consists of two terms: destruction by SN feedback in GMCs included in simulations and, additionally, destruction in the diffuse ISM by single SNe. The latter is implemented in a simplified way for all gas particles with $n_{\text{H}} < 1 \text{ cm}^{-3}$ assuming a constant destruction timescale of $\tau_{\text{dest}}^{\text{diff}}$, which can be expressed as

$$\tau_{\text{dest}}^{\text{diff}} = \frac{f_{\text{diff}} \Sigma_{\text{gas}}}{m_{\text{cl}} R_{\text{SN}}^{\text{diff}}}, \quad (19)$$

where f_{diff} is the mass fraction of the diffuse gas determined from the simulations and $R_{\text{SN}}^{\text{diff}}$ is the rate of SNe that explode in the diffuse gas. We assume $R_{\text{SN}}^{\text{diff}} = 8 \times 10^{-12} \text{ pc}^{-2} \text{ yr}^{-1}$. Numerically, we have $f_{\text{diff}}(n_{\text{H}} < 1 \text{ cm}^{-3}) = 0.35$. Note that the destruction timescale of all dust in the diffuse medium $\tau_{\text{dest}}^{\text{diff}}$ is shorter than the total destruction timescale in the entire ISM given by Equation (6).

The dependence of m_{cl} on density n_{H} is considered in Appendix A. To examine how this dependence affects our results, we run test simulations of dust evolution using the fitting formula for $m_{\text{cl}}(n_{\text{H}})$ given by Equation (24) in the expression for dust destruction rates. We find that the differences compared to the models with the fixed m_{cl} constitute less than 1%. We therefore adopt a fixed value of m_{cl} derived for a typical density in the diffuse gas of 0.1 cm^{-3} .

We name the models ECMRN x nm following ZDJ16, where x is the minimum grain size in nm and MRN indicates that all models assume an MRN grain size distribution. ‘‘E’’ and ‘‘C’’ in the name denote the enhanced collision rates due to Coulomb interactions and additional destruction in the diffuse ISM, respectively.

In the following, we apply the dust evolution model to determine the characteristics of grain populations that are responsible for the observed differences in the $[\text{Fe}_{\text{gas}}/\text{H}]$ and $[\text{Si}_{\text{gas}}/\text{H}]$ depletion levels in the ISM.

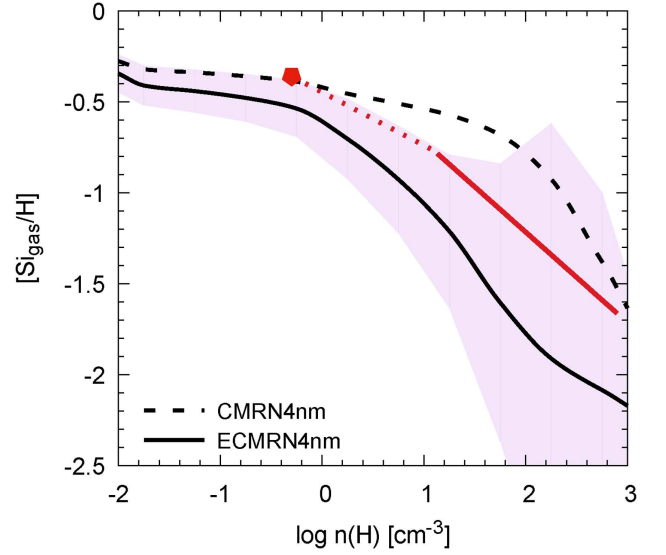


Figure 4. Relation between mean Si depletion and gas density derived from the final spatial distribution of gas-phase Si abundance in simulations and its standard deviation (ECMRN4nm; solid black line and a shadow area around it, respectively). The relation for the model without enhanced collision rates (CMRN4nm; dashed line) is shown for comparison. Observational data are the same as in Figure 3.

4.2. Silicon

Here we briefly summarize the model for silicate dust and refer to ZDJ16 for details. We model silicate evolution as traced by the Si abundance. To convert the Si abundance to the dust mass, we adopt amorphous silicates with olivine stoichiometric ratios. The dust evolution calculations start with homogeneous dust distribution with $[\text{Si}_{\text{gas}}/\text{H}] = -0.5$ or 68% of Si in dust. The total Si abundance $\epsilon_{\text{Si}} = 3.548 \times 10^{-5}$ (Asplund et al. 2009).

We estimate the destruction timescale in the diffuse gas from Equation (19) assuming a fixed value $m_{\text{cl}} = 1500 M_{\odot}$ (Zhukovska 2008), which results in the timescale of destruction in the diffuse gas $\tau_{\text{dest}}^{\text{diff}} = 220 \text{ Myr}$. The timescale of silicate dust destruction in the entire ISM equates to about 350 Myr in the steady state between destruction and growth of dust in the ISM. The slope of the observed $[\text{Si}_{\text{gas}}/\text{H}]-n_{\text{H}}$ relation is best reproduced with $a_{\text{min}} = 4 \text{ nm}$ and $a_{\text{max}} = 250 \text{ nm}$. These grain size limits are in excellent agreement with the classical MRN size distribution. The average grain radii are $\langle a \rangle_3 = 32$ and $\langle a^m \rangle_3 = 5.6 \text{ nm}$, without and with the account of Coulomb focusing, respectively. For a typical density and gas temperature in the CNM ($n_{\text{H}} = 30 \text{ cm}^{-3}$ and $T_{\text{gas}} = 100 \text{ K}$), the corresponding timescales of silicate dust growth are 15 and 1 Myr.

Figure 4 shows the relation between the mean $[\text{Si}_{\text{gas}}/\text{H}]$ and n_{H} predicted by the model and the relation inferred from observations in the local Milky Way. It is computed for the final distribution of gas and dust within a ring with galactic radii from 6 to 9 kpc that represents the conditions similar to the solar neighborhood. The mean $[\text{Si}_{\text{gas}}/\text{H}]$ is derived as described in ZDJ16 using mass-weighted probability density functions. In this work, the probability distribution functions are constructed for the linear depletion instead of the logarithmic depletion. For this reason the slopes of the relation shown in Figure 4 are somewhat shallower than those presented by ZDJ16 in their Figure 8.

4.3. Iron

4.3.1. Model Parameters

The iron element abundance in the Sun is similar to that of Si. Therefore, $[\text{Fe}_{\text{gas}}/\text{H}]$ values are expected to be similar to those of $[\text{Si}_{\text{gas}}/\text{H}]$, if Fe is also accreted on the silicate grains and Si and Fe have similar sputtering rates in SN shocks, $[\text{Fe}_{\text{gas}}/\text{H}]$ values should be similar to those of $[\text{Si}_{\text{gas}}/\text{H}]$. ZDJ16 found that the depletion levels in the WNM are determined by the destruction rates, while the depletions at high densities are controlled by the accretion rate. In order to reproduce the heavy depletion of interstellar Fe in the cold medium, we need a higher accretion rate of gas-phase Fe than that on the silicate grain surfaces. It can be provided if Fe is accreted on a population of small grains, as has been shown for another heavily depleted element Ti (Weingartner & Draine 1999).

Hensley & Draine (2017) recently demonstrated that even a large population of metallic iron nanoparticles with sizes down to 4.5 Å can be a viable component of the interstellar grains. We therefore include a population of metallic nanoparticles that accrete Fe from the gas phase and are destroyed by interstellar shocks. The size distribution of such grains is unknown. We assume a power-law size distribution with the lower size limit $a_{\text{min}} = 1$ nm and the upper size limit $a_{\text{max}} = 10$ nm, resulting in the mean particle size $\langle a \rangle_3 = 3.2$ nm. This is 10 times smaller than for silicate grains.

The fraction of iron in nanoparticles required to match $[\text{Fe}_{\text{gas}}/\text{H}] = -1.11$ in the WNM depends critically on the rate of destruction of iron dust. The latter is determined by the efficiency of metallic iron destruction as a function of shock velocity through Equation (23) for m_{cl} . Unfortunately, extensive theoretical studies of grain destruction in SN blast waves do not provide such data for metallic iron (Jones et al. 1994, 1996). Because small grains are sputtered in interstellar shocks more efficiently than large grains, we adopt the same value of $1500 M_{\odot}$ as for silicates, as a lower limit for m_{cl} . As we illustrate in the following section, even this low value of m_{cl} results in too high destruction rates and, respectively, too high $[\text{Fe}_{\text{gas}}/\text{H}]$ values in the WNM, if all solid Fe is placed in nanoparticles.

We consider two solutions to mitigate this discrepancy. The first solution assumes a two-component iron dust model, in which Fe resides in metallic nanoparticles and as metallic inclusions in other grains, for example, Mg-rich silicate grains. Existence of metallic inclusions in Mg-rich silicates is supported by X-ray observations in the CNM (Costantini et al. 2012). Such inclusions may form when iron nanoparticles stick on the silicate grains and are subsequently covered by silicate layers in the process of accretion and, at higher gas densities, coagulation of silicate grains. Nondetection of iron dust in Type Ia SNe, the major source of iron in the universe, suggests an interstellar origin of most of the solid iron as opposed to thermal condensation in the cooling circumstellar shells and SN ejecta (see also Dwek 2016). This is corroborated by recent microgravity experiments (Kimura et al. 2017) that find a low condensation efficiency of metallic iron at high temperatures.

We make a key assumption that the metallic inclusions are protected inside of these grains from rapid destruction by interstellar shocks. The inclusions will be eventually exposed to the surface as the layers covering them are sputtered away.

In this way, destruction may be the process that releases iron nanoparticles back to the diffuse gas and thus increases the surface area available for the subsequent accretion in the cold phase. A certain fraction of iron inclusions should also be destroyed, but we currently neglect this destruction term, assuming that it is small. We leave more detailed modeling of iron cycle in and out of silicate grains for future studies.

A fixed fraction of iron locked in silicates η_{Fe} is adopted here, for which we take the value of 0.7 used in a new model of interstellar silicates by Jones et al. (2013). Although the destruction timescale of free-flying nanoparticles is short ($\tau_{\text{dest}}^{\text{diff}} = 220$ Myr), the average timescale of destruction of iron dust $\tau_{\text{dest}}^{\text{ISM}} = 900$ Myr is longer than that for silicates because of the second iron dust component, metallic inclusions. This is our reference model.

Another scenario, in which all solid iron resides in free-flying metallic nanoparticles, requires the destruction of these particles to be less efficient than that of silicates to match the depletion in the WNM. It is hard to justify this scenario given that postshock velocities of iron grains are 15%–35% higher than equivalent silicate grain velocities (Jones et al. 1994). We examine the value of m_{cl} needed to fit $[\text{Fe}_{\text{gas}}/\text{H}]$ in the WNM for the case when all solid iron resides in nanoclusters.

In order to compute the mean grain radius modified by Coulomb focusing $\langle a^m \rangle_3$, we adopt the charge distribution functions for iron nanoparticles computed by Hensley & Draine (2017). The same as for silicates, we consider the iron dust growth only at temperatures below 300 K and compute the enhancement coefficient $D(a)$ for the grain charge distribution in the CNM. The majority of iron nanoparticles in the CNM have zero charge. However, a substantial fraction of iron nanoparticles has a negative charge of -1 : 0.36, 0.31, and 0.20 for particle sizes of 1, 5, and 10 nm, respectively. We find that the collision rate between gas-phase iron and metallic nanoparticles is significantly enhanced by Coulomb focusing on these negatively charged grains, resulting in $\langle a^m \rangle_3 = 0.038$ nm. This process decreases the timescale of growth of metallic grains in the CNM by a factor of 84, from 14 to 0.16 Myr, respectively, estimated for typical conditions in the CNM ($n_{\text{H}} = 30 \text{ cm}^{-3}$, $T_{\text{gas}} = 100$ K).

The electron field emission from negatively charged grains can be important for smaller grain sizes, since the critical grain charge for this process decreases with the grain size as $Z_{\text{d}(\text{cr})} \approx -210(a/100)^2$ (Tielens 2010). For the lower size limit adopted in this work, the critical grain charge is $Z_{\text{d}(\text{cr})} = -2.1$. The negative grain charge attained in the CNM is -1 , which is higher than $Z_{\text{d}(\text{cr})}$, and we can safely assume that electron field emission is not important in calculations of the accretion rates.

The simulations of iron dust evolution begin with the homogeneous iron abundance distribution, with $[\text{Fe}_{\text{gas}}/\text{H}] = -1.25$ corresponding to the Fe depletion in diffuse gas. As the dust evolves, the average $[\text{Fe}_{\text{gas}}/\text{H}]$ distribution more strongly correlates with the gas density owing to accretion of gas-phase Fe on grains until the system reaches a steady state between destruction and accretion in the ISM.

4.3.2. Variation of $[\text{Fe}_{\text{gas}}/\text{H}]$ with Gas Density

Figure 5 shows the synthetic mean $[\text{Fe}_{\text{gas}}/\text{H}] - n_{\text{H}}$ relation computed for the final spatial iron dust distribution for the reference model ECMRN1nm. Model CMRN1nm without

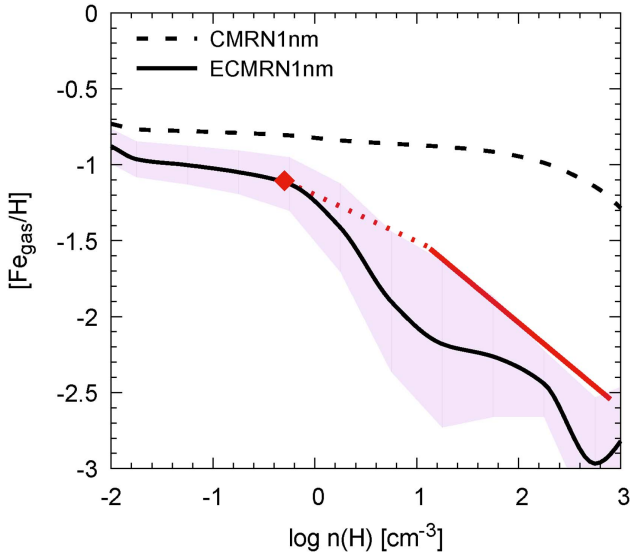


Figure 5. Same as Figure 4, but for iron gas-phase abundance $[\text{Fe}_{\text{gas}}/\text{H}]$ derived for reference model ECMRN1nm. The relation for the model without Coulomb focusing (CMRN1nm; dashed line) is shown for comparison. Observational data for $[\text{Fe}_{\text{gas}}/\text{H}]$ are the same as in Figure 3.

Coulomb focusing is shown for comparison. The adopted size distribution for iron nanoparticles in model ECMRN1nm with the Coulomb focusing provides a high accretion rate of gas-phase iron and, correspondingly, a steep slope similar to the observed $[\text{Fe}_{\text{gas}}/\text{H}] - n_{\text{H}}$ relation. The effective destruction timescale $\tau_{\text{dest}}^{\text{ISM}} = 900$ Myr, on the other hand, sets the $[\text{Fe}_{\text{gas}}/\text{H}]$ level in the low-density region. We did not vary the uncertain size distribution of nanoparticles to improve the fit to the observed relation.

Figure 6 shows the interstellar iron abundance in the gas phase $[\text{Fe}_{\text{gas}}/\text{H}]$ as a function of hydrogen column density of the gas N_{H} from simulations for reference model ECMRN1nm and that from observational data from Voshchinnikov & Henning (2010). $[\text{Fe}_{\text{gas}}/\text{H}]$ and N_{H} are calculated within 100 pc sized cells in the directions perpendicular to the disk plane. The model can reproduce well the flattening of $[\text{Fe}_{\text{gas}}/\text{H}]$ at low N_{H} and the decreasing trend for $N_{\text{H}} > 10^{20} \text{ cm}^{-2}$. Thus, our simulations agree with the observational data for $[\text{Fe}_{\text{gas}}/\text{H}]$ as a function of both column hydrogen density characterizing integrated properties of the ISM on the line of sight and the local density n_{H} . Large scatter in the predicted $[\text{Fe}_{\text{gas}}/\text{H}]$ values reflects different complex dynamical histories of the gas with the same N_{H} .

We also test two alternatives for the iron-containing dust component: (i) a case without nanoparticles, in which iron accretes on the silicate grain population described in Section 4.2; and (ii) a case with pure Mg-rich silicates with all iron in solid form residing in nanoparticles (Figure 7). Both models assume the same m_{cl} as for silicate grains. Model (i) fails to achieve the observed high Fe depletion level in the CNM. This is explained by a lower total surface area and, consequently, an accretion rate compared to the reference model with nanoparticles. The amount of depleted Fe is limited by the timescales of formation of GMCs, which in this case are shorter than the accretion timescales. Model (ii) can provide sufficiently fast growth and reproduce both the observed level of Fe depletion in the CNM and the slope of the $[\text{Fe}_{\text{gas}}/\text{H}] - n_{\text{H}}$ relation, but it overpredicts $[\text{Fe}_{\text{gas}}/\text{H}]$ in the WNM. During

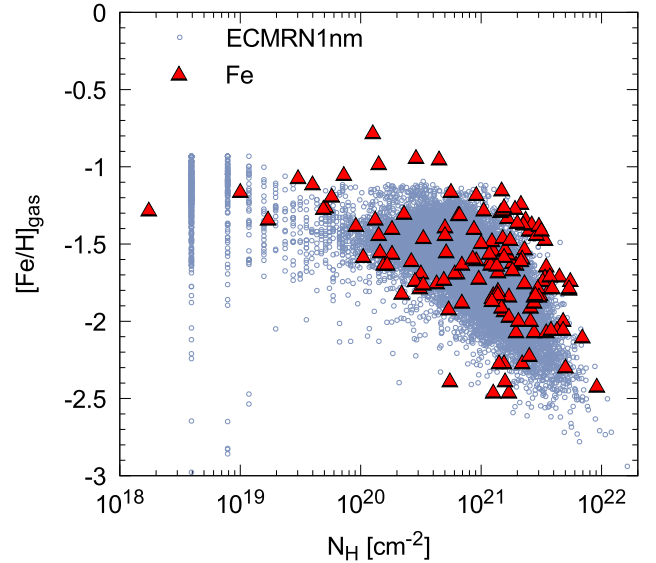


Figure 6. Interstellar Fe abundances as a function of hydrogen column density for reference model for iron dust evolution ECMRN1nm (circles) calculated within 100 pc sized cells in the direction perpendicular to the disk plane. Triangles show the values from observations (Voshchinnikov & Henning 2010).

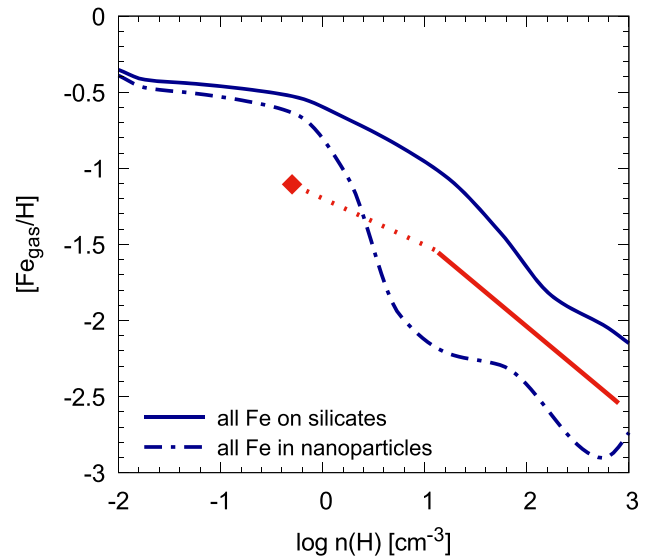


Figure 7. Relations between mean $[\text{Fe}_{\text{gas}}/\text{H}]$ and gas density derived from the final spatial $[\text{Fe}_{\text{gas}}/\text{H}]$ distributions for two test simulations: (i) a case without iron nanoparticles, in which iron accretes on the silicate grain population (solid line); and (ii) a case of pure Mg-rich silicates with all solid iron residing in the form of metallic nanoparticles (dot-dashed line). Only calculations that account for Coulomb focusing are shown.

their residence in the diffuse gas, grains are too efficiently destroyed, so that $[\text{Fe}_{\text{gas}}/\text{H}]$ remains on the level of -0.5 .

Model (ii), in which all solid iron is in free-flying nanoparticles, can match the $[\text{Fe}_{\text{gas}}/\text{H}]$ value in the WNM, if a longer timescale of destruction $\tau_{\text{dest}}^{\text{diff}} = 1.1$ Gyr is adopted. This value seems unrealistically high, since it is unlikely that iron nanoparticles are destroyed five times less efficiently than silicate grains, given that postshock velocities of iron grains are 15%–35% higher than equivalent silicate grain velocities (Jones et al. 1994).

5. How Do Grains Grow?

In this section we consider physical processes on the grain surface that may enable incorporation of new atoms into the solid. Chemical kinetics of the surface reactions leading to the growth of species of interests at low temperatures is yet to be understood and studied experimentally. The majority of experimental work on silicate condensation is conducted at high temperatures (~ 1000 K), with only a few recent experiments so far that considered formation of silicate materials at temperatures below 15 K (Krasnokutski et al. 2014; Rouillé et al. 2014; Henning 2017). They find no activation energy barrier for the chemical reaction of low-temperature silicate formation. Nucleation and growth of Fe nanoclusters and deposition of Fe metallic films on various surfaces have been extensively studied around room temperature and above (e.g., Wastlbauer & Bland 2007; Lübber et al. 2011, and references therein). Temperatures of iron grains in the diffuse medium are colder for most of time, but they increase drastically owing to stochastic heating by UV photon absorptions (Draine & Anderson 1985). Stochastic heating of dust grains probably plays an important role in the formation of distinct silicate and carbon grain populations (Serra Díaz-Cano & Jones 2008; Draine 2009), but the unknown binding energies for the species of interests (Si, Mg, Fe) on the surface of interest (silicates and metallic iron) are still the main hindrance for modeling these processes in detail. We consider the timescales of relevant processes and their possible roles in the dust growth in the diffuse ISM.

An impinging atom is initially bound by weak van der Waals forces to the surface. Our main assumptions are that (1) the surface has active sites, i.e., sites with dangling bonds and high binding energy, and (2) the growth occurs when an adsorbed atom reaches an active site. Surface diffusion enables the transport of adatoms to the sites with high binding energy. The time to scan the entire surface by this process is

$$\tau_{\text{sca}}^{-1} \approx N_s^{-1} \nu_0 \exp(-E_d/k_B T_d), \quad (20)$$

where E_d is the diffusion energy, T_d is the dust temperature, and N_s is the number of sites of the grain; $N_s = 4\pi a^2 n_s$, where $n_s \approx 1.5 \times 10^{15} \text{ cm}^{-2}$ is the surface density of physisorption sites (Hasegawa et al. 1992). Note that for $a = 1$ nm N_s is only 188, while it is 10^6 for a “classical” grain of $0.1 \mu\text{m}$. The diffusion energy is poorly known. Experimental work suggests that it is a fraction of the binding energy E_b of the adatom to the surface; we adopt $E_d = 0.3E_b$ here (Hasegawa et al. 1992).

Thermal desorption is the process that can remove an adsorbed atom from the grain surface before it reaches an active site. The timescale of thermal desorption is

$$\tau_{\text{des}}^{-1} \approx \nu_0 \exp(-E_b/k_B T_d), \quad (21)$$

where $\nu_0 \approx 10^{12} \text{ s}^{-1}$ is the vibrational frequency of the sticking species.

Both timescales τ_{sca} and τ_{des} are very sensitive to the binding energy. The value of E_b depends on many factors, including the chemical composition of the solid and its surface structure, in particular, on the number of unsatisfied bonds (Cuppen et al. 2017). We take heuristic values for E_b/k_B of 2700 K for Si and 4200 K for Fe from Hasegawa & Herbst (1993).

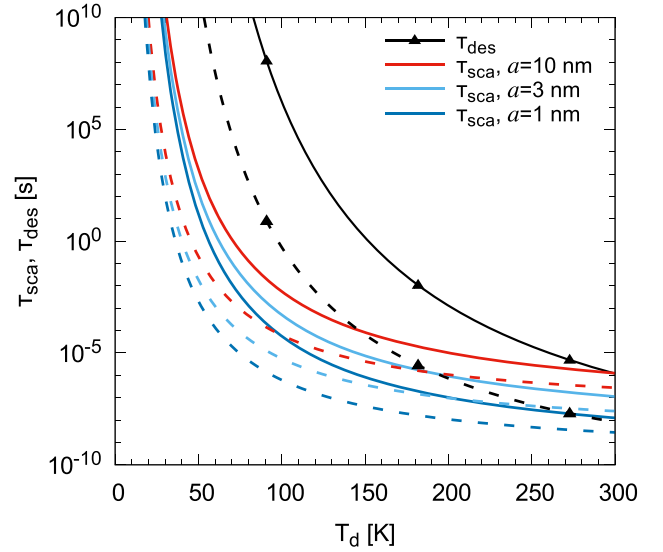


Figure 8. Scanning timescales τ_{sca} for grains with radii of 10, 3, and 1 nm (red, light-blue, and dark-blue lines, respectively) as a function of the grain temperature. Solid and dashed lines depict the timescales for $E_b/k_B = 4200$ K for Fe and 2700 K for Si, respectively. Desorption timescales τ_{des} are shown with black solid lines with filled triangles.

These values are similar to the physisorption energies estimated for water ice on silicate surface (Stimpfl et al. 2006).

Figure 8 shows the timescales of desorption and scanning for Fe and Si atoms on grains with radii of 1, 3, and 10 nm. Both species exhibit a large range of dust temperatures, for which $\tau_{\text{sca}} < \tau_{\text{des}}$. In this range, adsorbed atoms can scan the entire grain surface and find the sites with high binding energy before they are removed by thermal desorption. For $a = 10$ nm iron grains the scanning is faster than the thermal desorption for the dust temperatures up to 300 K and even higher for smaller sizes. In the following we consider temperatures of nanoparticles due to the stochastic heating.

Role of stochastic heating. The temperature of small grains in the standard interstellar field fluctuates compared to the equilibrium value, because the cooling timescale for these grains is shorter than the mean time between consecutive absorptions of UV photons (Draine & Anderson 1985). The maximum temperature T_{max} reached as a result of stochastic heating is determined by absorption of the maximum photon energy of 13.6 eV. For the smallest 1 nm spherical iron grains considered in this work, the equilibrium temperature is 50 K, while the actual T_d can rise to $T_{\text{max}} = 270$ K (Fischera 2004). Heating to these temperatures reduces the scanning time for Fe adatoms to $\lesssim 10^{-7}$ s (Figure 8). The stochastic heating may therefore play an important role for the iron growth in the diffuse ISM. This holds only if the time τ_{rad} needed for a grain heated to the temperature T_d to cool by emitting radiation is longer than the scanning timescale $\tau_{\text{sca}}(T_d)$.

In order to check this condition, we estimate the radiative cooling time for iron nanograins, applying for them the formalism introduced by Draine & Li (2001) for silicate and PAH particles. Draine & Li (2001) represent a small grain with N_a atoms as a vibrational system with $3N_a - 6$ degrees of freedom. The cooling time τ_{rad} for a grain with vibrational energy E_u gained by the absorption of an UV photon ($E_u = h\nu$)

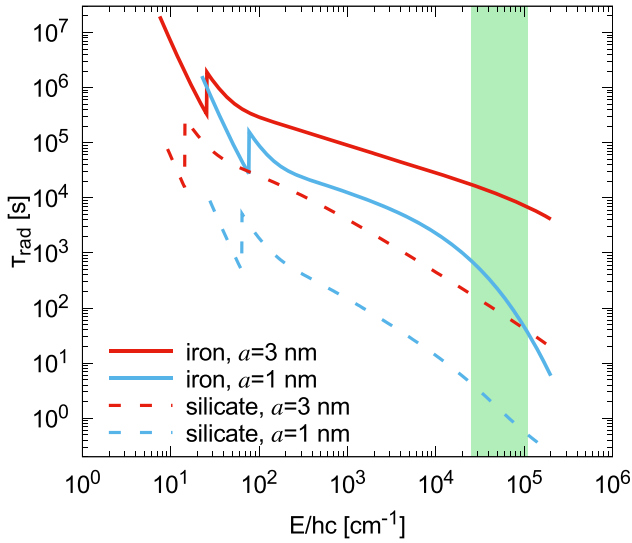


Figure 9. Radiative cooling time τ_{rad} as a function of vibrational energy E for iron grains with radii 3 and 1 nm (solid red and blue lines, respectively). The same for silicate grains is shown with dashed lines for comparison. The rectangle indicates the UV wavelength range of the interstellar radiation field.

is then determined by its absorption coefficient Q_{abs} :

$$\tau_{\text{rad}}(E_u) \approx \left[\frac{1}{E_u} \frac{8\pi^2 a^2}{h^3 c^2} \int_0^{E_u} \frac{E^3 Q_{\text{abs}}(E)}{\exp(E/kT_u) - 1} dE \right], \quad (22)$$

where T_u is the temperature of the vibrational system with energy E_u in the notations of Draine & Li (2001). It corresponds to the grain temperature T_d in our notations. The calculation of T_u and adopted data are briefly outlined in Appendix B.

The cooling timescales calculated from Equation (22) for iron and silicate grains are shown in Figure 9 as a function of the absorbed photon energy. We show $\tau_{\text{rad}}(E)$ for the grain sizes of 1 and 3 nm. The lowest values of τ_{rad} are derived for the maximum photon energy of 13.6 eV of the interstellar UV field and equal to 30 and 7000 s for 1 and 3 nm sized iron grains, respectively. Silicate particles have lower values of τ_{rad} , 0.5 and 38 s, respectively. This is the consequence of the higher opacities of silicates at long wavelengths ($\lambda \gtrsim 1 \mu\text{m}$) compared to iron grains.

The dust temperature rise from the UV absorption and consequently the reduction of τ_{sca} decreases rapidly with the particle size. For example, for 3 nm sized iron grains $T_{\text{max}} = 70$ K; the corresponding value of $\tau_{\text{sca}}(70 \text{ K}) = 0.11$ s is significantly longer than 3×10^{-8} s for 1 nm sized particle, but it is still shorter than the cooling time $\tau_{\text{rad}} = 7000$ s. It is the particles of this size and smaller that have the largest total surface area and a higher fraction of negatively charged grains; therefore, they are responsible for most of the iron dust production in our simulations. The role of stochastic heating on the growth is expected to diminish for larger particles.

We estimate the mean time between UV photon absorptions τ_{abs} to be equal to 1.2 and 35.5 days for iron particle sizes of 3 and 1 nm, respectively. Comparing these times to the time for radiative cooling, we find that small iron grains remain cool for most of the time, in agreement with other studies of thermal behavior of metallic grains (Tabak 1987; Fischera 2004; Hensley & Draine 2017). It is thus more likely that Fe atoms are accreted on cool grains and remain on the surface, since the probability of sticking is higher for lower T_d . In the proposed

picture of the dust growth, an accreted species can be delivered to an active site during the next UV absorption. The total number of such absorptions is 3×10^9 and 10^8 for 3 and 1 nm sized grains, respectively. It is estimated for the mean residence time of grains in the cold medium inferred from high-resolution hydrodynamic simulations and is equal to 10 Myr (Peters et al. 2017). These numbers of absorptions are orders of magnitude higher than the number of Fe atoms accreted by iron grains. We therefore conclude that the stochastic heating may indeed assist in the growth of small iron grains in the cold ISM.

6. Discussion

One-zone dust evolution models frequently assume that dust growth takes place in molecular clouds, because their high densities result in short timescales of accretion onto existing grains (e.g., Dwek 1998; Hirashita 2000; Zhukovska et al. 2008). The main difficulty with silicate dust growth in molecular clouds, as summarized by Jones & Nuth (2011) and Ferrara et al. (2016), is that under such conditions grains accrete not only silicate-forming elements but also abundant C-containing species (CO, CO₂, and other molecules) and H₂O that cover dust surfaces with ice mantles. Mantles have very different optical properties from the refractory dust materials required by the observed extinction features. Moreover, ice mantles are weakly bound to the grain surfaces and rapidly evaporate as grains return to the diffuse medium (Cuppen & Herbst 2007). Thus, volatile mantles cannot replenish diffuse gas with dust upon disruption of molecular clouds and explain element depletion patterns and dust masses in galaxies. While refractory carbonaceous materials may be formed upon irradiation of ice mantles by UV photons (Jenniskens et al. 1993), explaining the formation of amorphous silicates in molecular clouds remains problematic.

The models for silicate and iron dust evolution presented in this work show that efficient growth of these dust components commences in the diffuse gas, specifically in its cold neutral component. The rate of dust production by this mechanism is 20 times higher than the total rate of dust injection by stars (ZDJ16). Previous works found that the accretion timescale for grains with a “classical” radius of $0.1 \mu\text{m}$ is long compared to the residence time in the diffuse phase (Ferrara et al. 2016). This discrepancy is solved if we consider a grain size distribution including small grains. Because a fraction of small grains are negatively charged and species of interest are ionized (Fe, Si) in the CNM (Weingartner & Draine 1999; Yan et al. 2004), the collision rates of ions with grains are enhanced by Coulomb focusing. Assuming an MRN size distribution with a lower grain size of 4 nm for silicate grains and accounting for the enhanced collision rate, we find the timescales of accretion in the CNM that are shorter than the residence time in this phase. For iron grains, we need to extend the grain size distribution down to 1 nm to explain the higher depletion of gas-phase Fe compared to Si.

Temperature fluctuations of small grains due to the heating by interstellar UV photons may be vital for the dust growth, as shown in Section 5. The increase in the grain temperature drastically reduces the scanning time for an adsorbed species, permitting it to reach a site with high binding energy before this species is removed from the surface by thermal desorption.

Dust growth in the diffuse ISM allows us to explain the reformation of distinct populations of silicate and carbonaceous grains, in contrast to the mantles grown in molecular clouds. Irradiation of grains by the UV photons plays a key role in the

selective growth of silicate and carbonaceous grains as separate species (Draine 1990, 2009). It is based on the assumption that the binding energy of carbon atoms on the silicate grain surface is smaller than that of Mg, Si, Fe, and O; therefore, C can be cleared from their surfaces by photodesorption. Recent experimental work on the condensation of Si, O, Mg, and Fe on the low-temperature substrate indicates that these species are indeed able to react without an activation energy barrier. They form siliceous material that remains stable at room temperature and shows a $10\ \mu\text{m}$ spectral band, which is very similar to the silicate absorption feature observed in the ISM (Krasnokutski et al. 2014; Rouillé et al. 2014). Recent experiments have demonstrated that even in a situation where one starts with mixed precursors one gets separate silicate and carbonaceous particles (Henning 2017).

In the standard interstellar UV radiation field, Coulomb interactions enhance collision rates and enable dust growth by accretion at densities as low as $n_{\text{H}} \gtrsim 1\ \text{cm}^{-3}$. It is, however, noteworthy that physical conditions for dust growth in early star-forming galaxies are likely very different. In regions with a strong radiation field, dust grains are charged positively and Coulomb repulsion may hamper dust growth (Ferrara et al. 2016). Moreover, the ISM of galaxies forming stars at a 100 times higher rate than our own is expected to be highly turbulent. To discern whether dust growth is a viable source in the early universe requires better understanding of grain charging and matter cycle under extreme ISM conditions and is the subject of our future studies.

7. Conclusions

The interstellar abundance of refractory elements indicates substantial depletion that increases with gas density. Our new dust evolution model based on hydrodynamic simulations of the life cycle of GMCs established that the observed relation between the mean gas-phase Si abundance $[\text{Si}_{\text{gas}}/\text{H}]$ and the local gas density n_{H} is driven by a combination of selective silicate dust growth by accretion and efficient destruction in the diffuse ISM (ZDJ16). The model naturally includes different residence times of grains in interstellar phases and dependence of dust growth on the local density and temperature of the gas. In this work, we reinforce this conclusion with a simple analytic model for the Si depletion assuming a steady state between destruction and production of dust by stellar sources and by accretion in the ISM. We demonstrate that dust production by stars cannot reproduce the mean $[\text{Si}_{\text{gas}}/\text{H}] - n_{\text{H}}$ relation even for optimistic assumptions for the condensation efficiencies and the absence of dust destruction in SN shocks. This analytic model illustrates how the dependence of accretion timescale on gas density determines the negative slope of the $[\text{Si}_{\text{gas}}/\text{H}] - n_{\text{H}}$ relation.

We extend the framework developed in our previous work for silicates to include the evolution of iron dust, using the average $[\text{Fe}_{\text{gas}}/\text{H}] - n_{\text{H}}$ relation inferred from observations as the main constraint for the iron grain population. In order to explain a 0.9 dex lower value of $[\text{Fe}_{\text{gas}}/\text{H}]$ in the CNM compared to the $[\text{Si}_{\text{gas}}/\text{H}]$ value, we need a population of free-flying metallic nanoparticles with radii from 1 to 10 nm. However, if all iron missing from the gas resides in nanoparticles and their destruction is similar to that of silicate grains, the model overpredicts the $[\text{Fe}_{\text{gas}}/\text{H}]$ in the WNM by 0.5 dex compared to the observed depletion. The slope of the $[\text{Fe}_{\text{gas}}/\text{H}] - n_{\text{H}}$ relation is steeper than the observed value. This discrepancy is solved if we assume that 70% of the depleted

iron resides in the form of metallic inclusions inside of silicate grains, where it is protected from rapid destruction by interstellar shocks. Alternatively, the observed depletion trend can be described with a model in which all depleted Fe resides in nanoparticles, with the condition that their destruction efficiency is five times lower than that of the silicate grain population. Such low destruction of metallic nanoparticles is currently difficult to reconcile with predictions by theoretical models for dust destruction in interstellar shocks.

Enhanced collision rates due to the electrostatic focusing in the CNM are crucial for both silicate and iron dust models to reproduce the slope of the observed depletion–density relations and the magnitude of depletions at high densities. Without taking the grain charges into account, the timescales of accretion are longer than the timescale of formation of GMCs, and the resultant $[\text{X}_{\text{gas}}/\text{H}]$ values in the CNM are higher than the observed values.

We consider the timescales of relevant physical processes for adsorbed Si and Fe atoms on the grain surfaces. A process that is currently not included in the dust evolution models but may be important for the dust growth is stochastic heating of small grains by UV photon absorption. We demonstrate that the timescale for radiative cooling of a grain after an absorption is longer than the timescale for scanning of the surface by an adsorbed species. The increase in the grain temperature drastically reduces the scanning time and enables delivery of adsorbed species to the sites with high binding energy.

We thank an anonymous referee for helpful comments that improved the clarity of the paper. S.Z. acknowledges support by the Forschungsgemeinschaft through SPP 1573: “Physics of the Interstellar Medium.” We gratefully acknowledge the Max Planck Computing and Data Facility for providing their user support and computing time on the Odin and Hydra clusters.

Appendix A

Density Dependence of Dust Destruction

The quantity $m_{\text{cl},j}$ is determined by the properties of the dust material and the structure of the blast wave

$$m_{\text{cl},j}(n_0) = \int_{v_0}^{v_f} \epsilon_j(v_s, n_0) \left| \frac{dM_s(v_s, n_0)}{dv_s} \right| dv_s, \quad (23)$$

where v_0 and v_f are the initial and final velocities of the supernova remnant (SNR) expanding into an ambient medium of density n_0 , respectively, $\left| \frac{dM_s(v_s, n_0)}{dv_s} \right| dv_s$ is the mass of gas swept up by a shock with velocity in the range of $[v_s, v_s + d v_s]$, and ϵ_j is the efficiency of dust destruction in an SN shock with expansion velocity v_s . We calculate $\left| \frac{dM_s(v_s, n_0)}{dv_s} \right|$ using an analytical solution for the SNR evolution expanding in a homogeneous medium from McKee (1989). The solution combines the adiabatic expansion and pressure-driven snowplow stages. We adopt an expression for $\epsilon_j(v_s, n_0)$ for silicate dust calculated by Jones et al. (1996), which is available only for the ambient density $n_0 = 0.25\ \text{cm}^{-3}$. Although the efficiency of dust destruction in an SN shock depends on the density of the ambient medium (Jones et al. 1994, 1996; Nozawa et al. 2006), it should not significantly vary in the density range of $0.2\text{--}1\ \text{cm}^{-3}$, which encompasses 70% of the diffuse gas in our simulations. We derive the following quadratic fitting formula for

this integral for metallicity $Z = 0.014$:

$$m_{\text{cl},j}(n_0) = a(\log n_0)^2 + b \log n_0 + c, \quad (24)$$

where $a = 22$, $b = -305.85$, and $c = 1438.93$ for silicate dust. This formula is accurate within 1% with respect to the numerical integration of Equation (24).

Appendix B Stochastic Heating of Nanoparticles

In order to calculate the radiative cooling time for an iron grain upon absorption of a photon (Equation (22)), we apply a statistical-mechanical description of the emission process (Draine & Li 2001). A grain with N_a atoms is approximated as a vibrational system with $N_m = 3N_a - 6$ degrees of freedom. The main assumptions of this approach are that (1) the energy of the absorbed photon $h\nu$ is distributed ergodically among these degrees of freedom before any infrared emission and (2) the absorption coefficient is independent of the degree of excitation. An assumption that the vibrational modes of the grain are approximated by harmonic oscillators allows us to calculate the temperature T_u of grains in the excited state $E_u = h\nu$ from the equation $\bar{E}(T) = E_u$, where \bar{E} is the expectation value for the vibrational energy:

$$\bar{E}(T) = \sum_{j=1}^{N_m} \frac{\hbar\omega_j}{\exp(\hbar\omega_j/kT) - 1}, \quad (25)$$

where ω_j is the fundamental frequency of the mode j . We adopt an n -dimensional Debye spectrum for the fundamental modes for silicate and iron grains described respectively in Draine & Li (2001) and Hensley & Draine (2017).

For metallic iron, we adopt $Q_{\text{abs}}(a, \lambda)$ from Fischera (2004), who calculated the optical properties of spherical pure iron grains using Mie theory for wavelengths $2\pi a/\lambda > 0.1$ and dipole approximation at longer wavelengths. Optical properties for astronomical silicates are taken for silicate grains (Draine & Lee 1984; Laor & Draine 1993).

ORCID iDs

Svitlana Zhukovska  <https://orcid.org/0000-0003-2569-3627>

References

- Altobelli, N., Postberg, F., Fiege, K., et al. 2016, *Sci*, 352, 312
Aoyama, S., Hou, K.-C., Shimizu, I., et al. 2017, *MNRAS*, 466, 105
Asplund, M., Grevesse, N., Sauval, A. J., & Scott, P. 2009, *ARA&A*, 47, 481
Barlow, M. J., Krause, O., Swinyard, B. M., et al. 2010, *A&A*, 518, L138
Bate, M. R., Bonnell, I. A., & Price, N. M. 1995, *MNRAS*, 277, 362
Bekki, K. 2015, *MNRAS*, 449, 1625
Benz, W., Cameron, A. G. W., Press, W. H., & Bowers, R. L. 1990, *ApJ*, 348, 647
Bevan, A., Barlow, M. J., & Milisavljevic, D. 2016, *MNRAS*, 465, 4044
Bianchi, S., & Schneider, R. 2007, *MNRAS*, 378, 973
Bilalbegovic, G., Maksimovic, A., & Mohacek-Grosecv, V. 2017, *MNRAS*, 466, L14
Costantini, E., Pinto, C., Kaastra, J. S., et al. 2012, *A&A*, 539, A32
Cuppen, H. M., & Herbst, E. 2007, *ApJ*, 668, 294
Cuppen, H. M., Walsh, C., Lamberts, T., et al. 2017, *SSRv*, 212, 1
de Looze, I., Barlow, M. J., Swinyard, B. M., et al. 2017, *MNRAS*, 465, 3309
Dobbs, C. L., & Pringle, J. E. 2013, *MNRAS*, 432, 653
Dorschner, J., & Henning, T. 1995, *A&ARv*, 6, 271
Draine, B. T. 1990, in ASP Conf. Ser. 12, The Evolution of the Interstellar Medium, ed. L. Blitz (San Francisco, CA: ASP), 193
Draine, B. T. 2009, in ASP Conf. Ser. 414, Cosmic Dust—Near and Far, ed. T. Henning, E. Grün, & A. Steinacker (ASP: San Francisco, CA), 453
Draine, B. T., & Anderson, N. 1985, *ApJ*, 292, 494
Draine, B. T., & Hensley, B. 2013, *ApJ*, 765, 159
Draine, B. T., & Lee, H. M. 1984, *ApJ*, 285, 89
Draine, B. T., & Li, A. 2001, *ApJ*, 551, 807
Dwek, E. 1998, *ApJ*, 501, 643
Dwek, E. 2004, *ApJL*, 611, L109
Dwek, E. 2016, *ApJ*, 825, 136
Dwek, E., & Scalo, J. M. 1980, *ApJ*, 239, 193
Ferrara, A., Viti, S., & Ceccarelli, C. 2016, *MNRAS Letters*, 463, L112
Fischera, J. 2004, *A&A*, 428, 99
Gail, H.-P., Zhukovska, S., Hoppe, P., & Trieloff, M. 2009, *ApJ*, 698, 1136
Gioannini, L., Matteucci, F., Vladilo, G., & Calura, F. 2017, *MNRAS*, 464, 985
Gomez, H. L., Krause, O., Barlow, M. J., et al. 2012, *ApJ*, 760, 96
Hasegawa, T. I., & Herbst, E. 1993, *MNRAS*, 261, 83
Hasegawa, T. I., Herbst, E., & Leung, C. M. 1992, *ApJS*, 82, 167
Henning, T. 2017, in IAU Symp., Astrochemistry VII, ed. Maria Cunningham et al. (Cambridge: Cambridge University Press), in press
Henning, T., Begemann, B., Mutschke, H., & Dorschner, J. 1995, *A&AS*, 112, 143
Hensley, B. S., & Draine, B. T. 2017, *ApJ*, 834, 134
Hirashita, H. 2000, *PASJ*, 52, 585
Indebetouw, R., Matsuura, M., Dwek, E., et al. 2014, *ApJL*, 782, L2
Jenkins, E. B. 2009, *ApJ*, 700, 1299
Jenkins, E. B., & Tripp, T. M. 2011, *ApJ*, 734, 65
Jenniskens, P., Baratta, G. A., Kouchi, A., et al. 1993, *A&A*, 273, 583
Jones, A., Tielens, A., & Hollenbach, D. 1996, *ApJ*, 469, 740
Jones, A. P., Fanciullo, L., Köhler, M., et al. 2013, *A&A*, 558, A62
Jones, A. P., & Nuth, J. A. 2011, *A&A*, 530, 44
Jones, A. P., Tielens, A. G. G. M., Hollenbach, D. J., & McKee, C. F. 1994, *ApJ*, 433, 797
Kimura, Y., Tanaka, K. K., Nozawa, T., Takeuchi, S., & Inatomi, Y. 2017, *SciA*, 3, 1
Krasnokutski, S. A., Rouillé, G., Jäger, C., et al. 2014, *ApJ*, 782, 15
Kroupa, P. 2002, *Sci*, 295, 82
Laor, A., & Draine, B. T. 1993, *ApJ*, 402, 441
Lübben, O., Krasnikov, S. A., Preobrajenski, A. B., Murphy, B. E., & Shvets, I. V. 2011, *Nano Research*, 4, 971
Mathis, J. S., Rumpl, W., & Nordsieck, K. H. 1977, *ApJ*, 217, 425
McDonald, I., Boyer, M. L., Van Loon, J. T., & Zijlstra, A. A. 2011, *ApJ*, 730, 71
McKee, C. 1989, in IAU Symp. 135, Interstellar Dust, ed. L. J. Allamandola & A. G. G. M. Tielens (Dordrecht: Kluwer), 431
McKinnon, R., Torrey, P., & Vogelsberger, M. 2016, *MNRAS*, 457, 3775
Micelotta, E. R., Dwek, E., & Slavin, J. D. 2016, *A&A*, 590, A65
Min, M., Waters, L. B. F. M., de Koter, A., et al. 2007, *A&A*, 462, 667
Nozawa, T., Kozasa, T., & Habe, A. 2006, *ApJ*, 648, 435
O'Donnell, J. E., & Mathis, J. S. 1997, *ApJ*, 479, 806
Ossenkopf, V., Henning, T., & Mathis, J. 1992, *A&A*, 261, 567
Peters, T., Zhukovska, S., Naab, T., et al. 2017, *MNRAS*, 467, 4322
Price, D. J., & Monaghan, J. J. 2007, *MNRAS*, 374, 1347
Rouillé, G., Jäger, C., Krasnokutski, S. A., Krebsz, M., & Henning, T. 2014, *FaDi*, 168, 449
Savage, B. D., & Bohlin, R. C. 1979, *ApJ*, 229, 136
Savage, B. D., & Sembach, K. R. 1996, *ARA&A*, 34, 279
Schalen, C. 1965, *PASP*, 77, 409
Serra Diaz-Cano, L., & Jones, A. P. 2008, *A&A*, 492, 127
Silvia, D. W., Smith, B. D., & Shull, M. J. 2010, *ApJ*, 715, 1575
Slavin, J. D., Dwek, E., & Jones, A. P. 2015, *ApJ*, 803, 7
Stimpff, M., Walker, A. M., Drake, M. J., de Leeuw, N. H., & Deymier, P. 2006, *JCrGr*, 294, 83
Tabak, R. G. 1987, *Ap&SS*, 134, 145
Tielens, A. G. G. M. 1998, *ApJ*, 499, 267
Tielens, A. G. G. M. 2010, The Physics and Chemistry of the Interstellar Medium (Cambridge: Cambridge Univ. Press)
Voshchinnikov, N. V., & Henning, T. 2010, *A&A*, 517, A45
Voshchinnikov, N. V., Henning, T., & Il'in, V. B. 2017, *ApJ*, 837, 25
Wastlbauer, G., & Bland, J. A. C. 2007, *AdPhy*, 54, 137
Weingartner, J., & Draine, B. 1999, *ApJ*, 517, 292
Westphal, A. J., Stroud, R. M., Bechtel, H. A., et al. 2014, *Sci*, 345, 786
Yan, H., Lazarian, A., & Draine, B. T. 2004, *ApJ*, 616, 895
Zhukovska, S. 2008, PhD thesis, Ruperto-Carola-Universität
Zhukovska, S., Dobbs, C., Jenkins, E. B., & Klessen, R. S. 2016, *ApJ*, 831, 147
Zhukovska, S., Gail, H.-P., & Trieloff, M. 2008, *A&A*, 479, 453
Zhukovska, S., Petrov, M., & Henning, T. 2015, *ApJ*, 810, 128
Zubko, V., Dwek, E., & Arendt, R. G. 2004, *ApJS*, 152, 211